Publisher's version: Tousignant, K. & Packer, J.A. (2017). Fillet weld effective lengths in CHS X-connections. I: Experimentation. Journal of Constructional Steel Research, 138: 420-431. https://doi.org/10.1016/j.jcsr.2017.08.005

Fillet Weld Effective Lengths in CHS X-Connections. I: Experimentation

Kyle Tousignant[a] and Jeffrey A. Packer[a*]

[a] Department of Civil Engineering, University of Toronto, 35 St. George Street, Toronto, ON, M5S 1A4, Canada

[*] Corresponding Author. E-mail: jeffrey.packer@utoronto.ca; Tel: +1-416-978-4776; Fax: +1-416-978-7046

Abstract

For the first time, an experimental test program was conducted to assess the strength of fillet welds in circular hollow section (CHS) connections. Six large-scale, fillet-welded CHS-to-CHS X-connections were designed with varied key parameters that affect the weld strength: branch-to-chord diameter ratio, chord wall slenderness, and branch inclination angle. By means of quasi-static tension applied to the branches, fracture of 12 test welds (two per connection) was obtained. Strain distributions measured adjacent to the welds indicated a weld effective length less than the total weld length, under pure axial load. Branch loads at rupture were also measured and used to determine the structural reliability of existing AWS provisions for weld effective lengths in CHS-to-CHS X-connections. For the range of parameters studied, the provisions are found to be very conservative. Hence, methods are assessed to accurately quantify the weld effective length. A parametric modelling study is presented in a companion paper to develop more liberal recommendations.

Key words

Hollow structural section, Circular hollow section, Fillet weld, Effective length, Connection, Experimentation

1. Introduction

When welding to hollow structural sections (HSS), welds can be proportioned: (a) to achieve the capacity of the connected branch member wall; or (b) to be “fit for purpose” [1]. By designing welds as “fit for purpose” – to resist the actual forces present in the branch member – smaller, more appropriate weld sizes typically result.

In order to account for the non-uniform loading of the weld perimeter due to differences in the relative flexibilities of the chord loaded normal to its surface, and the branch(es) carrying membrane stresses parallel to its surface, weld effective properties – including weld effective lengths and weld effective section moduli – are used. These properties are determined by discounting segments of the weld which do not contribute to its overall resistance. The weld effective length is hence less than or equal to the total weld length. Simply put, it is the amount of weld that can be relied upon to resist the loading on the connection.

Over the last 30 years, much research has been conducted at the University of Toronto to determine weld effective lengths for rectangular hollow section (RHS) connections, including gapped K-connections, T-, Y- and X- (or Cross-) connections, moment-loaded T-connections, and overlapped K-connections [2-6]. Recommendations based on this research have been adopted as code in North America, by the American Institute of Steel Construction (AISC) in Section K5: “Welds of Plates and Branches to RHS” of their latest specification, AISC 360 [7].

Since the addition of Section K5 (formerly Section K4, in the 2010 specification), weld effective properties for circular hollow section (CHS) connections have been an issue faced by code writers, including AISC and the American Welding Society (AWS), since load transfer around a welded CHS joint can be highly non-uniform [8] (e.g. Fig. 1).

While AISC [7] is noticeably silent regarding weld effective lengths for CHS connections, AWS D1.1 “Structural Welding Code – Steel” [9] implies, in Clause 9.6.1.3(4), that the weld effective length in axially loaded CHS connections is equal to 1/1.5 of the total weld length under factored loads, regardless of the joint geometry. While believed to be conservative, this rule is not supported by experimental evidence.

A laboratory-based test program was hence conducted to assess the performance of welds in CHS connections. For the first time, weld-critical tests (where failure occurs by weld fracture) have been completed on fillet welds in full-scale CHS connections, and the structural reliability (safety index) of the existing AWS, AISC and CSA specification provisions for the design of such welds is determined. The effect of key connection parameters on the weld strength is also investigated, and an empirical method to quantify the weld effective length is proposed. The results of this paper are vital for determining a strategy for the fit-for-purpose design of welds in CHS connections that is both accurate (reasonably predicts the correct failure load) and safe (meets or marginally exceeds target reliability indices provided by design codes).

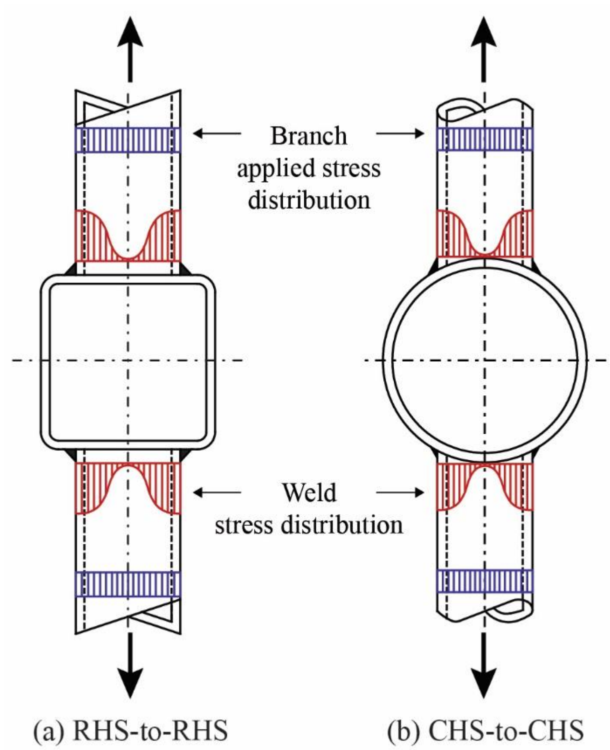

Fig. 1. Variation of X-connection stress distributions

2. Test specimen preparation and material testing

Six CHS X-connections were designed and fabricated from ASTM A500 [10] dual-certified Grade B/C cold-formed CHS, and fillet welded using a semi-automatic flux-cored arc welding (FCAW) process with full CO_2 shielding gas. As it was speculated that the strength of welds in CHS X-connections depends on branch-to-chord diameter ratio (β = D_b/D), chord wall slenderness (D/t), and branch inclination angle (θ), the chord and branch members were selected to cover a wide range of these values, as shown in Table 1. These values were selected to be within limits for fillet welds to develop the full throat thickness, as given by AWS [9] (see Section 2.1). Four connections had branches at 90° to the chord, and two connections had branches at 60° to the chord. The connection layout is shown in Fig. 2, which includes the nomenclature used herein.

Table 1

Measured properties of 12 CHS X- (test) connections

Test [a]	CHS branch member			CHS chord member			θ	β	D/t	τ	P_a [d]	P_a' [e]
	$D_b \times t_b$	A_b [b]	F_y [c]	$D \times t$	A [b]	F_y [c]						
	mm × mm	mm²	MPa	mm × mm	mm²	MPa	°				kN	kN
102-273-90a	102.0 × 7.34	2161	373	273.5 × 11.69	9614	460		0.37	23.4	0.63	672	672
102-273-90b	102.0 × 7.34	2161	373	273.5 × 11.69	9614	460		0.37	23.4	0.63	678	678
102-406-90a	102.0 × 7.34	2161	373	406.5 × 12.34	15283	355		0.25	32.9	0.59	608	608
102-406-90b	102.0 × 7.34	2161	373	406.5 × 12.34	15283	355	90	0.25	32.9	0.59	540	540
127-273-90a	127.4 × 11.55	4207	431	273.5 × 11.69	9614	460		0.47	23.4	0.99	653	653
127-273-90b	127.4 × 11.55	4207	431	273.5 × 11.69	9614	460		0.47	23.4	0.99	609	653
127-406-90a	127.4 × 11.55	4207	431	406.5 × 12.34	15283	355		0.31	32.9	0.94	557	557
127-406-90b	127.4 × 11.55	4207	431	406.5 × 12.34	15283	355		0.31	32.9	0.94	556	557
102-406-60a	102.0 × 7.34	2161	373	410.0 × 12.21	15260	373		0.25	33.6	0.60	721	721
102-406-60b	102.0 × 7.34	2161	373	410.0 × 12.21	15260	373	60	0.25	33.6	0.60	538	721
127-406-60a	127.4 × 11.55	4207	431	410.0 × 12.21	15260	373		0.31	33.6	0.95	761	761
127-406-60b	127.4 × 11.55	4207	431	410.0 × 12.21	15260	373		0.31	33.6	0.95	798	850

[a] In the test designation: the first number represents the nominal branch diameter; the second number represents the nominal chord diameter; the third number represents the branch inclination angle (θ); and a/b represent the side of the connection, since each connection had two fillet welds (a = top; b = bottom).

[b] Cross-sectional areas determined by cutting a prescribed length of CHS, weighing it, and then using a density of 7850 kg/m³ to calculate its cross-sectional area.

[c] Yield strength of all CHS determined from tensile coupon tests performed according to ASTM A370 [11] while maintaining the curved shape.

[d] Actual (experimental) weld fracture load.

[e] Greatest load sustained by the weld.

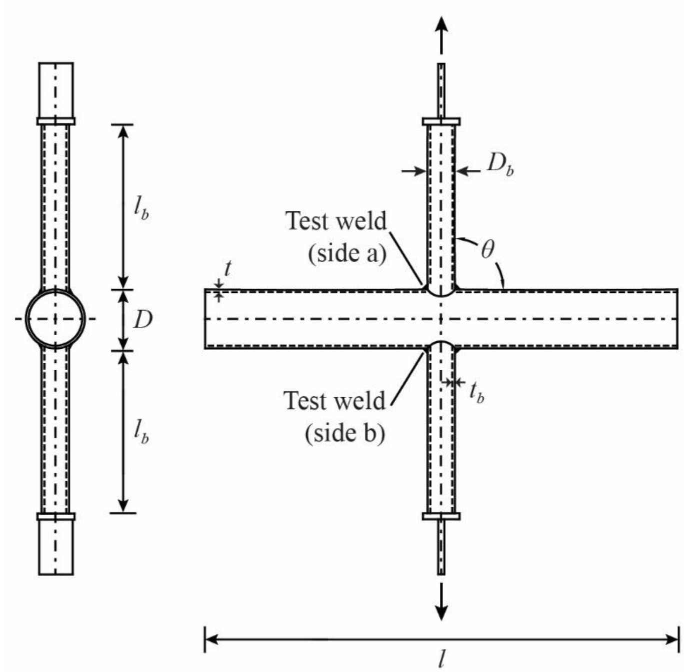

Fig. 2. Connection layout

2.1. Connection geometric considerations

CHS members and connection geometry had to be carefully designed, to maintain the local dihedral angle (Ψ) of the joints between 60° and 120°, to develop the full fillet weld throat thickness (t_w). According to Note 4 in Fig. 9.10 of AWS [9], when $\Psi < 60°$ the Z loss values in AWS [9] Table 9.5, for PJP welds, apply. To keep Ψ within this range, the complex effect of β and θ on Ψ, which changes continuously around the joint, was studied using the vector-calculus approach given by Luyties & Post [12]. Using a subtended angle increment ($\Delta\rho$) equal to 1°, as suggested by Luyties & Post [12], it was determined that β must not exceed 0.50 for 90° CHS connections, and 0.28 for 60° CHS X-connections.

While having θ less than 60°, and thus Ψ less than 60°, would adversely affect the weld strength by contributing to the Z loss (loss of the weld throat) at the root of the weld, according to Table 9.5 of AWS [9], having slightly larger β-values, and thus Ψ slightly greater than 120° does not. For the design of test connections it was therefore deemed necessary to keep θ between 60° and 90°, while a minor deviation from the stated β limits was considered acceptable. Local dihedral angle curves for each test connection showing the variation of Ψ along the weld length are shown in Fig. 3. These curves have been determined by applying the method given by Luyties

& Post [12] in Matlab, with $\Delta\rho$ equal to 1° and measured values of D_b and D. The letters "a" and "b" at the end of the test designation in Table 1 have been omitted since the curves apply to both branch connections on either side of the chord (i.e. "a" and "b"). Local dihedral angle curves for connections with different β values, calculated using the same method, have also been included in Fig. 3. These curves can be compared to those given in Informative Annex O of AWS [9] to verify the approach used.

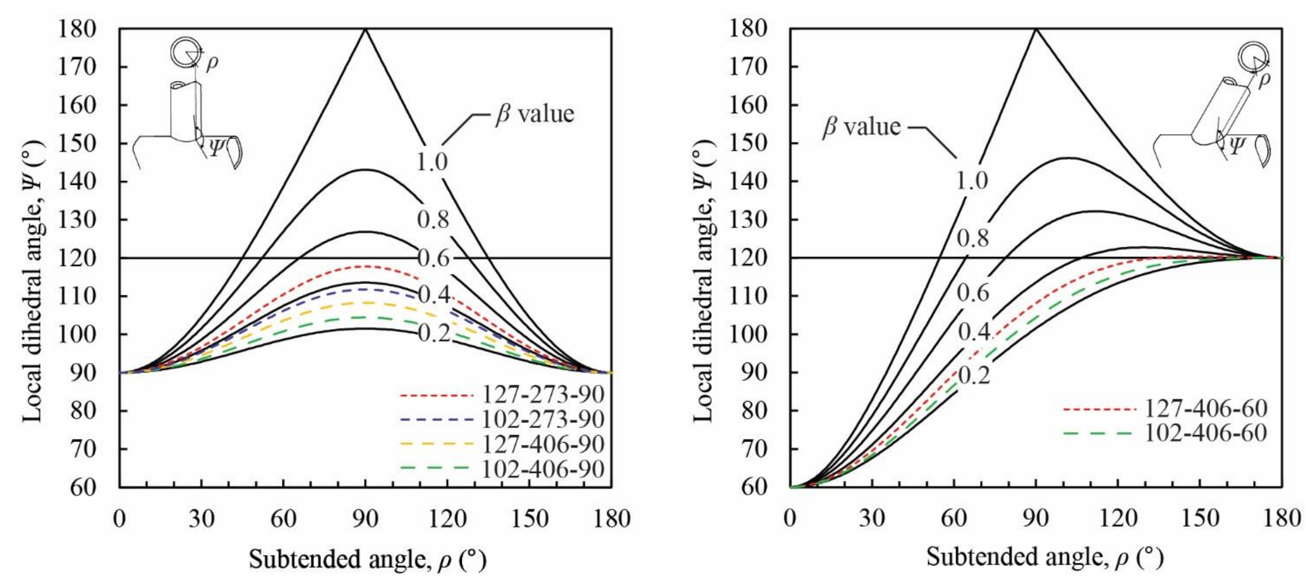

(a) θ = 90° connections (b) θ = 60° connections

Fig. 3. Local dihedral angle curves for test joints, with subtended angle measured from the crown heel

The branches were cut to a minimum branch length (l_b) of $6D_b$, to avoid shear lag effects at mid-length, from both ends [13], and profiled to saddle perfectly onto the chords, without edge bevelling (Fig. 4). The branches were capped by a tee connection through which load was applied. The tee connection was designed, using Section 7.6 of Packer & Henderson [14], to develop the member capacity. The chords were cut to an overall chord length (l) to avoid end effects at the connection [15]. To economize on material, they were left unrestrained (uncapped) at both ends. The average measured material properties for the CHS branch and chord members were determined from three tensile coupon tests per section, performed according to ASTM A370 [11] while maintaining the curved shape. One tensile coupon was taken from each CHS directly across from the weld seam, and the other two were taken from the CHS faces orthogonal to the weld seam.

(a) Typical 90° connection (shown for 102-273-90a) (b) Typical 60° connection (shown for 102-406-60b)

Fig. 4. Fit-up of branch to chord after profiling and tack welding

2.2. Geometrical properties of the as-laid welds

Correct measurement of the geometric properties of the welds, which comprise a complex saddle shape in CHS connections, is critical to the subsequent scientific analysis of the weld strength; hence, great care was taken to very accurately obtain these measurements.

The total weld length (l_w), and the weld length tributary to each throat size measurement (which is necessary to determine the average throat size for the joint), were calculated by modifying a vector-calculus approach used previously to determine Ψ by Luyties & Post [12] to give a near-perfect solution for the distance between points along the weld root, and then summing up these distances. This can be done using computer-programmed equations (e.g. in Matlab) as follows:

Step 1: Starting at a subtended angle (ρ) equal to 0° (i.e. the heel of the connection, Fig. 5a) (or the beginning of the interval of interest), compute the coordinates of the branch-chord intersection at ρ and $\rho + \Delta\rho$ using Eq. (1a). Eq. (1a) gives the position vector $\vec{P}_i$ at point i along the branch-chord intersection, where i equals ρ or $\rho + \Delta\rho$. The notation [( ), ( ), ( )] represents the three vector components in the branch coordinate system (Fig. 5b).

$$\vec{P}_i = [(l_t), \quad \left(\frac{D_b}{2}\sin i\right), \quad \left(\frac{D_b}{2}\cos i\right)] \tag{1a}$$

where:

$$l_t = \frac{D_b(1 - \cos i)}{2\tan\theta} + \frac{D - \sqrt{D^2 - (D_b \sin i)^2}}{2\sin\theta} \tag{1b}$$

Step 2: Calculate the vector ($\vec{V}$) connecting these points: $\vec{V} = \vec{P}_{\rho+\Delta\rho} - \vec{P}_{\rho}$.

Step 3: Compute the magnitude of $\vec{V}$ by taking the square root of the sum of squares of its three vector components. This is the approximation to the weld length between $\vec{P}_{\rho}$ and $\vec{P}_{\rho+\Delta\rho}$. The smaller $\Delta\rho$ is, the closer the approximation will be to the actual weld length.

Step 4: Increment ρ by $\Delta\rho$, and repeat Steps 1 to 3, adding the new result for the magnitude $\vec{V}$ to the previous results. For the total weld length, continue repeating Steps 1 to 3 until ρ is equal to 360° - $\Delta\rho$. For an interval length along the weld, continue repeating Steps 1 to 3 until ρ is exactly $\Delta\rho$ less than ρ at the end of the interval.

The weld lengths herein were calculated as described above with $\Delta\rho$ equal to 1°. This generally gave the same answer for total weld length as an exact solution based on calculus, but could be more easily applied to a range of different joint geometries. Lie et al. [16] also provided equations to describe the geometry of butt welds in HSS Y-connections. If used to calculate Ψ or l_w for the current tests, the results would match the Authors' because both approaches are based strictly on the connection geometry.

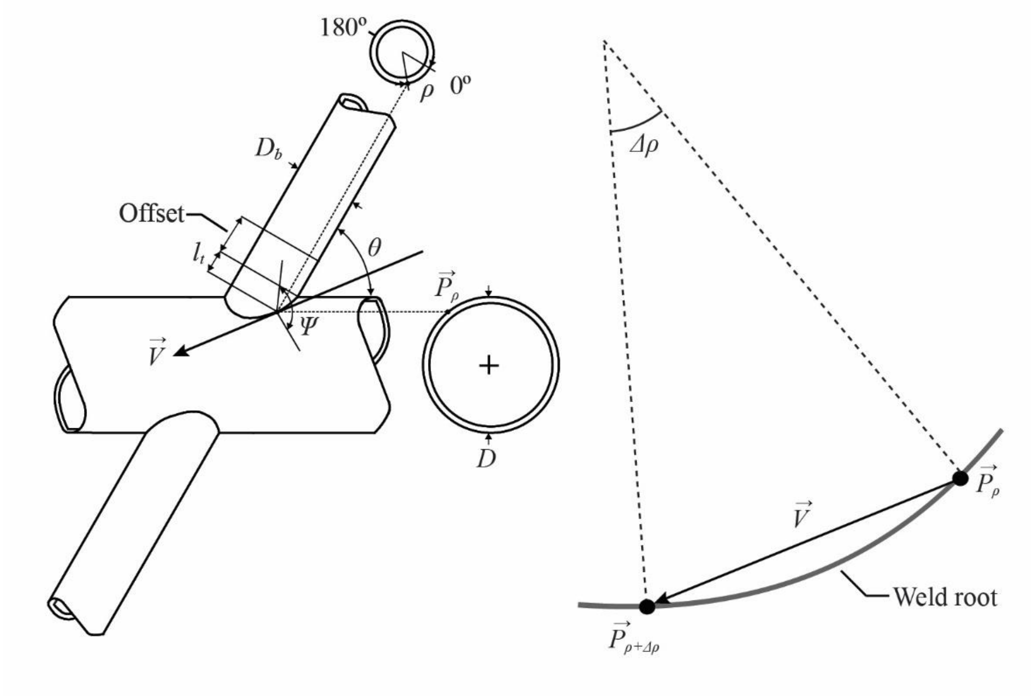

(a) scalar and vector parameters

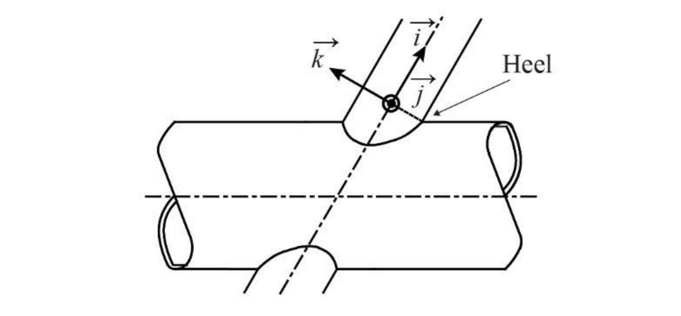

(b) branch coordinate system

Fig. 5. Vector calculus method used to determine weld lengths

After being laid, welds were ground into a triangular shape, with a near-uniform throat size (t_w) around each joint, and flat weld faces. Flat weld faces allowed t_w to be obtained from a 3D model of the weld's exact geometry, as shown in Fig. 6. Using this approach, the orientation of t_w and the weld legs (l_v and l_h) must be established correctly: in the plane of Ψ, perpendicular to the weld root, between tangents to the outside surfaces of the branch and the chord. The computer-aided design (CAD) program Solidworks was employed to exact this requirement.

First, local components of l_v and l_h in a plane containing the branch axis and the normal to the branch face were measured at uniform increments of ρ along the weld length. The component of l_v parallel to the branch was first measured by wrapping a mat board collar with reinforced edges around the branch at a fixed distance (or "offset") from the root of the weld at the heel of the connection. The offset distance (Fig. 5(a)) was then measured using a Mitutoyo Digimatic calliper (with a specified resolution of 0.01 mm). The distance between the collar and the weld toe along the branch (x) was then measured, using the same calliper, at uniform increments of ρ along the weld length. The component of l_v parallel to the branch at ρ could then be calculated by subtracting this measured distance (x) from the theoretical distance between the collar and the weld root (= l_t + offset). Historically, l_t refers to the template length, which is the length (parallel to the branch) of a steel-cutting template that was wrapped around a CHS branch and used as a guide for profiling with a torch. The component of l_h perpendicular to the face of the branch at ρ was measured by laying a standard fillet weld gauge along the axis of the branch and measuring the distance to the weld toe. The weld profile around the entire joint was then modelled in Solidworks using these measurements and the measured values of D_b and D. Finally, sections were taken through the weld in the plane of Ψ using Solidworks geometry tools, and l_v, l_h and t_w were precisely measured, as shown in Fig. 6.

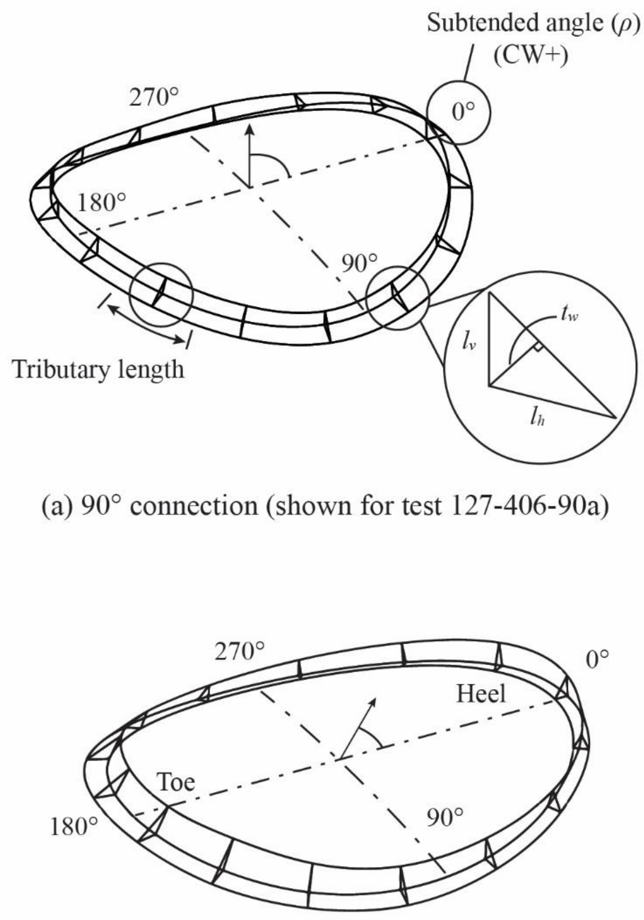

(a) 90° connection (shown for test 127-406-90a)

(b) 60° connection (shown for test 127-406-60b)

Fig. 6. 3D Solidworks models of weld profile and weld dimensions

The weld area (A_w) was determined by summing up: $t_w \times$ tributary weld length (Fig. 6) around the entire joint (weighted average). The measured fillet-weld geometric properties are shown in Table 2.

Table 2
Weld dimensions and predicted fracture loads for test joints according to existing AWS [9] provisions for weld effective lengths in CHS X-connections

Test	Average measured weld dimensions					P_n[a]
	l_v mm	l_h mm	t_w mm	l_w mm	A_w mm	kN
102-273-90a	6.86	6.17	4.08	322	1312	303
102-273-90b	7.23	6.65	4.37	322	1405	324
102-406-90a	5.16	5.78	3.56	320	1139	263
102-406-90b	4.54	5.08	3.14	320	1004	232
127-273-90a	5.94	5.93	3.63	406	1475	340
127-273-90b	7.05	6.06	4.00	406	1625	375
127-406-90a	4.83	5.03	3.16	403	1273	294
127-406-90b	5.60	5.19	3.47	403	1410	323
102-406-60a	5.83	5.59	3.58	345	1235	285
102-406-60b	6.29	5.83	3.79	345	1307	302
127-406-60a	5.68	8.01	3.95	434	1716	396
127-406-60b	5.39	6.00	3.38	434	1468	339

[a] Nominal predicted fracture load according to existing AWS [9] specification provisions, calculated using Eqs. (2a,b) and (3), using A_w and F_{EXX} determined from tensile coupon tests (= 577 MPa).

2.2.1. Post-rupture macro-etch examinations

To verify the values of l_v and l_h obtained using Solidworks, post-rupture macro-etch examinations of the fillet welds were performed after several tests. Four cross sections of the fillet weld profile (at ρ = 0°, 90°, 180°, and 270°) were cut in the plane of Ψ using a drop saw. The cross sections were then hand polished, macro-etched using a 5% nital etchant solution, and digitized at a scale of 1:1. Using the program AutoCAD, l_v, l_h, and t_w were re-measured from the cross sections. The weld throat (t_w) was taken as the shortest distance from the root to the face of the diagrammatic weld. The average value of t_w for the macro-etched connections was then determined, using a tributary width for each measurement equal to $0.25l_w$, and compared to the previous measurements. The mean ratio of the measurements (Solidworks/macro-etch) was found to be 0.96. The macro-etch weld leg measurements hence gave credence to the Solidworks-based dimensions derived from external caliper measurements, which are used herein.

2.3. Mechanical properties of the as-laid welds

The mechanical properties of the as-laid welds were determined by tensile coupon testing in accordance with AWS [9]. A summary of the all-weld-metal tensile coupon test results is given in Table 3.

Table 3
All-weld-metal tensile coupon test results

All-weld-metal coupon designation	Yield stress MPa	Young's modulus, E MPa	F_{EXX} MPa	Rupture strain, ε_{rup}[a] %
[i]	510	189000	573	30.6
[ii]	520	201000	576	27.4
[iii]	521	235000	581	26.4
Average	517	208000	577	28.1

[a] Rupture strain determined by re-joining the fractured coupon and measuring: change in gauge length / initial gauge length

The average yield stress from three coupon tests (by the 0.2% strain offset method) was 517 MPa and the average ultimate stress (F_{EXX}) was 577 MPa with 28.1% elongation at rupture. The measured ultimate strength was 17.8% greater than the specified nominal strength (490 MPa) of the E71T-1C electrode used. The welding process specifications used for the joints were: voltage = 25 V, amperage = 260 A, and travel speed = 230 mm/min. Welding was performed principally in the flat position, by a welder qualified with the Canadian Welding Bureau for the position and the FCAW process used.

3. Connection tests and instrumentation

Quasi-static axial tension load was applied to the end of each branch on either side of the connection, and hence to the weld, by a 2700-kN capacity universal testing machine (UTM). The typical testing arrangement is shown in Fig. 7.

Four linear strain gauges (SGs), equally spaced around the perimeter of the branch at mid length ($\geq 3D_b$ from the welded test joint and the end), and oriented along its longitudinal axis, were used to measure the uniformity of load being applied to the branch. Equal strains were typically measured at all four locations over all tests, indicating that axial load was predominantly applied.

Seven additional SGs, with the same orientation, were used around half the weld perimeter (i.e. on one side of the branch only, due to symmetry) to measure non-uniform loading of the weld perimeter (Fig. 8). For this purpose, SGs were centred 20 mm away from the weld toe, to avoid stress concentrations that occur there due to the notch effect [4], and located at ρ = 0°, 30°, 60°, 90°, 120°, 150°, and 180°. A single SG in the saddle position on the opposite side (at ρ = 270°) was used to verify symmetry of the strain distribution about the plane of the connection. In all, 12 welds were tested to rupture (two per connection). All welds failed in a brittle manner, by fracture along a plane through the weld. Four typical failures are shown in Fig. 9, for both 90° connections (Figs. 9a,b) and 60° connections (Figs. 9c,d).

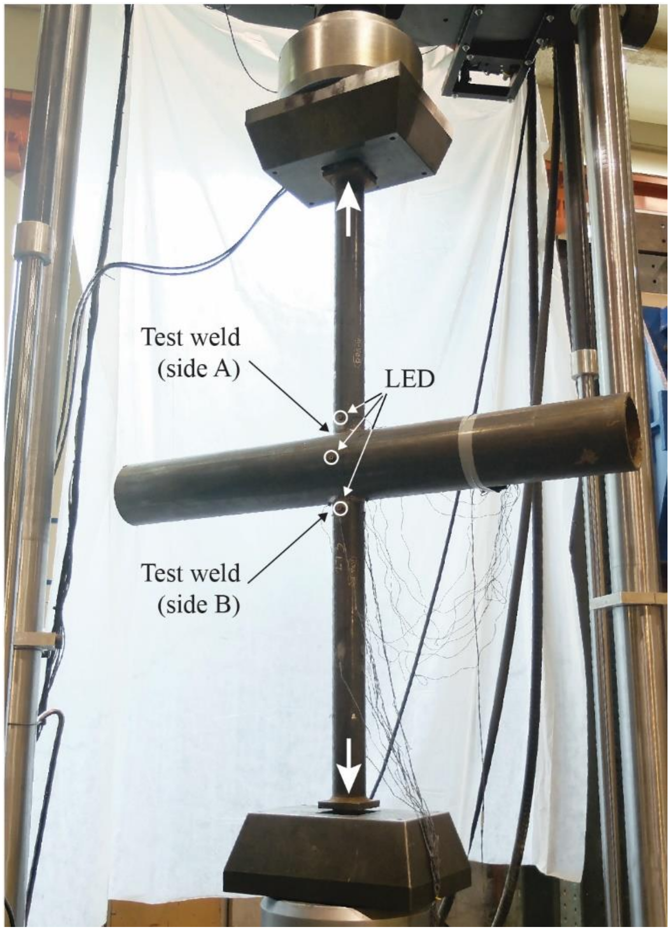

Fig. 7. Typical testing arrangement (shown for test 127-273-90a)

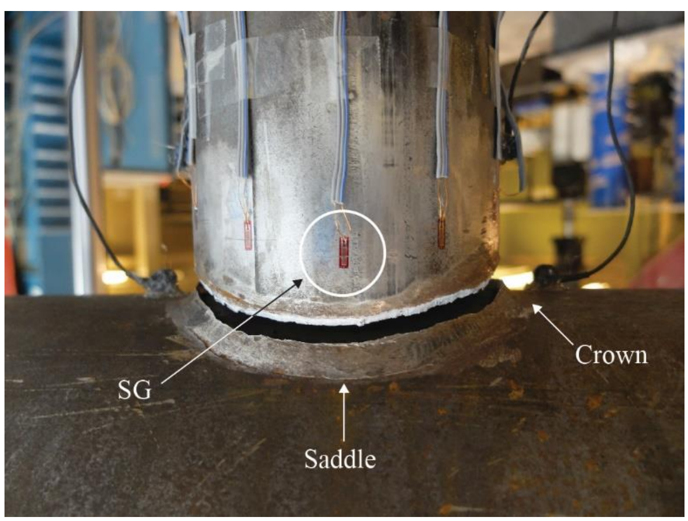

Fig. 8. Strain gauges near weld toe (and weld fracture) in test 127-273-90a

(a) Test 102-273-90a (θ = 90°)

(b) Test 127-406-90a (θ = 90°)

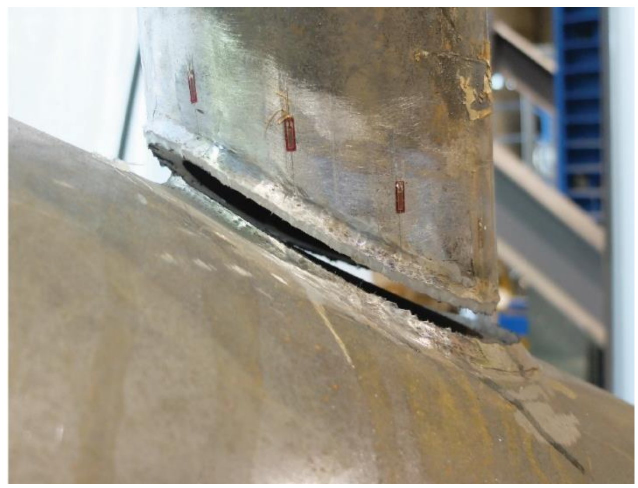

(c) Test 102-406-60a (θ = 60°)

(d) Test 102-406-60a (θ = 60°)

Fig. 9. Typical weld fractures

After the first test weld (e.g. side a) ruptured in each connection, the branch was re-positioned within the UTM and tack-welded back in place. The entire connection was then removed from the UTM, and fully re-welded (nominally in the flat position) to ensure separation of the same branch did not occur again. The connection was re-placed in the UTM, and tested until rupture of the second test weld (e.g. side b) occurred. Chord deformation (δ) was continuously monitored throughout both tests with three LED targets: one on each branch, 50-mm above the crown; and one at the connection work point on the chord face parallel to the plane of the connection (Figs. 7, 10). The value of δ, which is defined as the outward displacement, normal to the chord, of a single branch from the chord centreline [17], was taken as the normal component of half of the displacement between the LEDs on each branch (Fig. 10). It therefore represents the average deformation on both sides of the connection. The applied loads (and hence P_a and P_a' given in Table 1) were obtained from load cells in-line with the UTM actuator, and verified by comparison with forces computed from average SG readings of strain at mid-length of the branch and the measured branch cross-sectional area (A_b) and Young's modulus (E).

4. Discussion of results

4.1. Applied load versus deformation response

Fig. 10 shows the relationship between δ, expressed as a fraction of the chord diameter (δ/D), and the applied load (P) for several representative tests. The six curves shown on Fig. 10 correspond to the first weld tested on each connection (e.g. side a). To determine the relationship between δ/D and the applied load for the second tests, residual displacements from the first test needed to be taken into account. The residual displacements were estimated using an unloading curve with the same slope as the initial connection stiffness. This curve was projected back, from the point of rupture of the first test, onto the x-axis, as shown in Fig. 11. This marked the origin for the measured curve from the second test. The overall δ/D versus applied load response for the second test was then obtained by extending the corresponding first curve past its point of rupture until it met the second curve. This part of the curve is illustrated by the dashed black line in Fig. 11. The chord deformation at rupture (δ_a) for the six second welds tested (e.g. side b) could then be obtained. Despite having only small fillet welds, chord plastification in excess of the 3%D deformation limit [18] occurred before rupture in seven out of the 12 tests (Table 4).

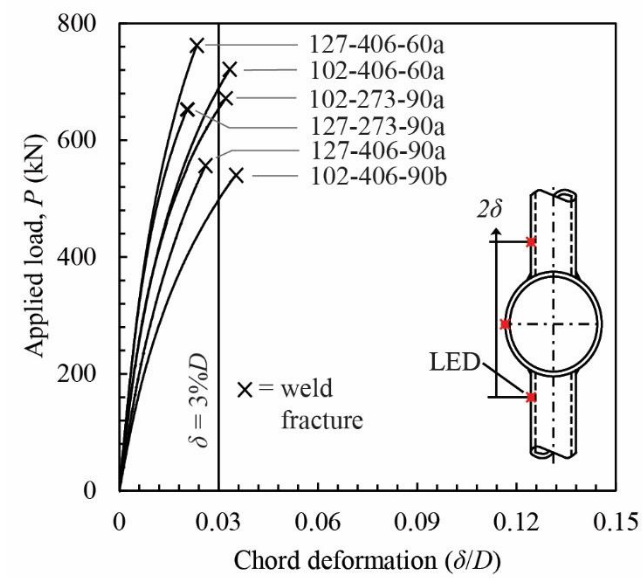

Fig. 10. Typical load versus chord deformation relationships

241

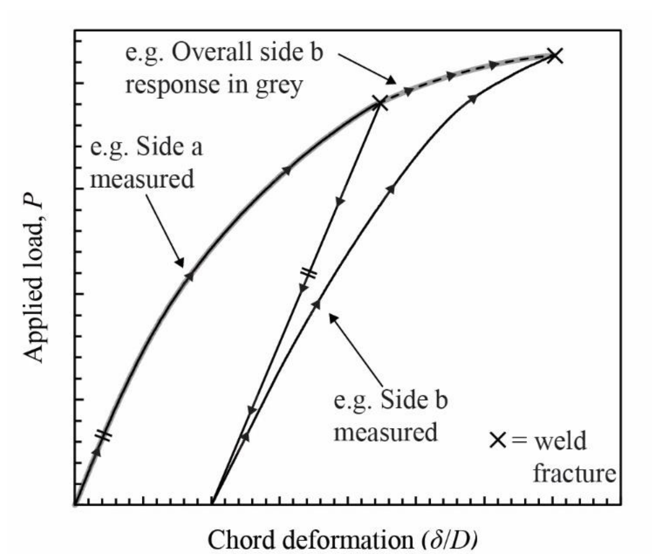

Fig. 11. Procedure for calculating load versus deformation for second welds tested

242

Table 4
Residual chord deformation (at start of test) and chord deformation at rupture for all 12 tests

Test	Residual chord deformation (as percent of *D*) %	δ_a/D %
102-273-90a	0	3.23
102-273-90b	1.732	3.68
102-406-90a	1.577	4.70
102-406-90b	0	3.52
127-273-90a	0	2.06
127-273-90b	0.914	2.07
127-406-90a	0	2.61
127-406-90b	0.962	2.78
102-406-60a	0	3.34
102-406-60b	1.759	3.63
127-406-60a	0	2.34
127-406-60b	1.712	3.60

Note: residual chord deformations are equal to zero for first weld tested on each connection

4.2. Non-uniform strain distributions adjacent to the weld

Representative graphs of the strain distribution around the branch adjacent to the test weld, at fractions of the actual (experimental) weld fracture load (P_a), are given in Figs. 12 and 13. Moreover, Figs. 12 and 13 present the strains measured during the test in which the corresponding weld actually fractured. It is shown that, for θ = 90° connections (Figs. 12a,b), the tensile strain (and hence tensile load) decreases as a function of distance away from the saddle (ρ = 90° point). The tensile strain is therefore smallest at the crown (ρ = 0° and 180° points), with much of the weld even remaining in compression for the entire tension load range. This phenomenon equates to a non-uniform loading of the weld perimeter – which is expectedly more pronounced for connections with higher β-values, where stiff membrane action dominates load transfer at the saddle. It can thus be concluded that weld effective lengths are present in CHS-to-CHS connections. An illustration of the effect that causes compression at the crown is shown in Fig. 14.

The largest tensile strains for θ = 60° connections were initially measured at the saddle (Figs. 13a,b). As the load increased, the strain adjacent to the saddle, on the heel side of the connection, began to increase at a faster rate than the strain adjacent to the saddle on the toe side of the connection. This is due to secondary bending effects from connection flexibility and joint rotation, which may not exist in real structures where the chord ends are prevented from rotating.

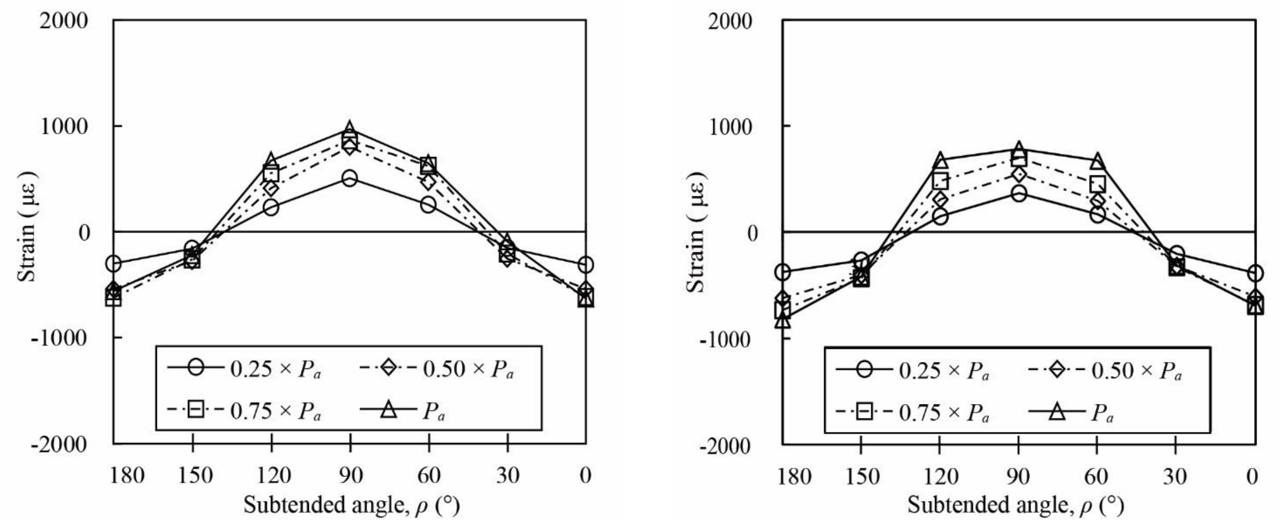

(a) Test 127-273-90a (β = 0.47, θ = 90^{o})　　(b) Test 127-406-90a (β = 0.31, θ = 90^{o})

Fig. 12. Typical strain distributions adjacent to test weld (θ = 90° connections)

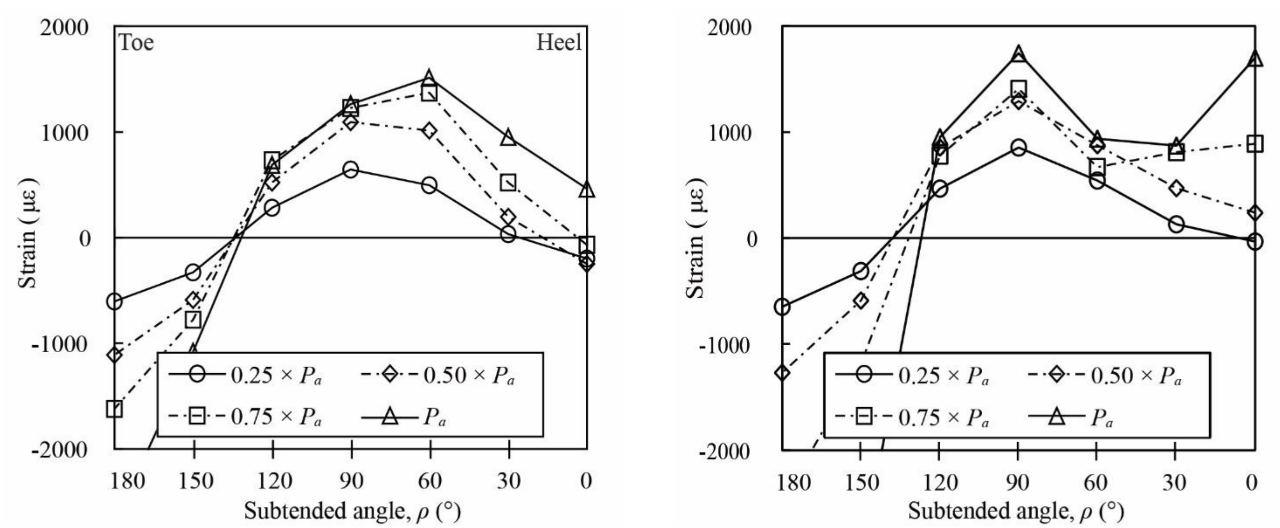

(a) Test 102-406-60a (β = 0.25, θ = 60^{o})　　(b) Test 127-406-60a (β = 0.31, θ = 60^{o})

Fig. 13. Typical strain distributions adjacent to test weld (θ = 60° connections)

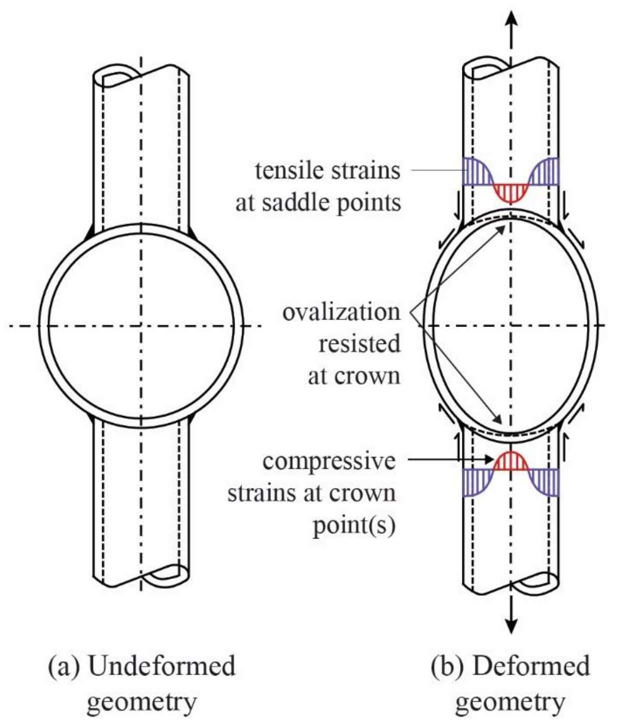

Fig. 14. Effect causing compressive strains at the crown (ρ = 0° and 180° points) (θ = 90° connections)

5. Evaluation of AWS [9]

5.1. Existing provisions for weld effective lengths in CHS X-connections

According to Clause 9.5.3 of AWS [9], the nominal strength of fillet welds in CHS X-connections designed as fit-for-purpose (P_n) is based on the limit state of shear rupture along the plane of the weld effective throat in accordance with Eqs. (2a,b):

$$P_n = Q_w l_e \tag{2a}$$

$$Q_w = 0.60 t_w F_{EXX} \tag{2b}$$

where l_e = weld effective length [9]. An LRFD resistance factor for fillet welds, ϕ, equal to 0.80, is then applied to determine the design strength.

In Clause 9.5.4, simplified equations are given to compute weld lengths for CHS connections under axial load, which can be traced back to Appendix C of British Standard 449 [19]. These factors can be shown to calculate the *total* weld length, rather than the *effective* weld length. A branch stress/load factor of 1.50 is specified by AWS, in Clause 9.6.1.3(4) “Uneven Distribution of Load (Weld Sizing)”, for design using the LRFD method. This factor, established in the 1980s, is used to prevent progressive weld failure due to non-uniform load transfer across the weld when welds are designed as fit-for-purpose. In modern day LRFD, the approach is to apply a reduction to the resistance of the weld, by calculating a weld effective length, rather than to increase the design load. Hence, it is deduced that the weld effective length implied by AWS Clause 9.6.1.3(4) is the inverse of the stress/load factor:

$$l_e = \frac{1}{1.5} l_w = \frac{2}{3} l_w \tag{3}$$

5.2. Safety level inherent in AWS [9]

To assess whether adequate or excessive safety margins are inherent, the structural reliability (or safety index) (β^+) can be calculated and compared to the minimum target value in North America (4.0, as currently adopted by AISC [7] per Section B3.1 of the AISC [7] Commentary), using a reliability analysis in which the resistance factor, ϕ, is given by Eq. (4) [20, 21]:

$$\phi = \phi_{\beta^+} \rho_R \exp\left[-\alpha_R \beta^+ V_R\right] \tag{4}$$

where α_R = coefficient of separation taken as 0.55 [20]; ρ_R = bias coefficient for resistance; V_R = associated coefficient of variation (COV) of ρ_R; and $\phi_\beta{}^+$ = adjustment factor for β^+ that is needed when $\beta^+ \neq 3.0$ [21]. The bias coefficient for resistance (ρ_R) and its associate COV (V_R) are given by Eqs. (5) and (6):

$$\rho_R = \rho_M \rho_G \rho_P \tag{5}$$

$$V_R = \sqrt{V_M^2 + V_G^2 + V_P^2} \tag{6}$$

where ρ_M = mean ratio of actual-to-nominal electrode strength; ρ_G = mean ratio of actual-to-nominal weld throat area; ρ_P = mean test-to-predicted capacity ratio (with predicted capacity calculated using actual measured properties); and V_M, V_G, and V_P = COV of ρ_M, ρ_G, and ρ_P, respectively.

A formula to calculate $\phi_\beta{}^+$ based on the reliability index (β^+) was derived by Franchuk et al. [22]:

$$\phi_{\beta^+} = 0.0062(\beta^+)^2 - 0.131\beta^+ + 1.338 \tag{7}$$

The mean actual-to-nominal electrode strength (ρ_M) and its associated COV (V_M) were taken from a database of 708 tests summarized in Table 5. The data from recent University of Toronto test programs in Table 5 are average values from tensile coupon tests done for studies by McFadden & Packer [5], Tousignant & Packer [6, 23], and the current study (recall that the measured electrode strength was 17.8% greater than the specified nominal strength). The composite mean and COV of all test data were used for ρ_M and V_M, respectively.

Table 5
Mean actual-to-nominal electrode strength (ρ_M) and associated variation (V_M) amongst typical weld metal

Study	Number of tests	ρ_M	V_M
Lesik & Kennedy [24]	672	1.12	0.077
Callele et al. [25]	32	1.15	0.080
Recent University of Toronto test programs (including current work)[a]	4	1.21	0.039
Composite/total values:	708	1.12	0.121

[a] nominal electrode strength is assumed to be 490 MPa for all electrodes tested.

The mean measured-to-nominal weld throat area (ρ_G) and its associated COV (V_G) were taken as 1.03 and 0.10, respectively [25]. These factors account for the fact that larger weld throats are typically provided by convexity of the weld face. They do not account for the use of the simplified equations in AWS [9] to compute weld lengths for CHS connections under axial load. This is discussed in Section 5.4.

The mean test-to-predicted capacity ratio (ρ_P) was taken as the average over all tests of P_a' (Table 1) divided by P_n (Table 2), with P_n calculated using Eqs. (2a,b) and (3), and the measured values of A_w and F_{EXX}. The reliability analysis parameters, and the results of the reliability analysis, are shown in Table 6.

Table 6
Reliability analysis parameters

	AWS [9]		AISC [7]	CSA [26]
l_e/l_w	2/3	unity	unity	unity
ϕ	0.80	0.80	0.75	0.67
ρ_M	1.12	1.12	1.12	1.12
V_M	0.12	0.12	0.12	0.12
ρ_G	1.03	1.03	1.03	1.03
V_G	0.10	0.10	0.10	0.10
ρ_P	2.13	1.42	1.42	1.27
V_P	0.13	0.13	0.13	0.13
ρ_R	2.48	1.65	1.65	1.47
V_R	0.21	0.21	0.21	0.21
ϕ_{β^+}	0.72	0.85	0.82	0.82
β^+	7.0	4.9	5.2	5.2

The implied safety index, β^+, is equal to 7.0 for the existing AWS [9] specification provisions, which is much larger than the minimum target safety index of 4.0 in North America. This indicates that a high level of conservatism is present in the AWS formulae. Fig. 15 shows the correlation of the existing AWS predicted nominal strengths with the experimental results. The actual strength in Fig. 15 is taken as the greatest load sustained by the weld (P_a'), from Table 1. On average, the actual strength is 2.13 times larger than that predicted by AWS.

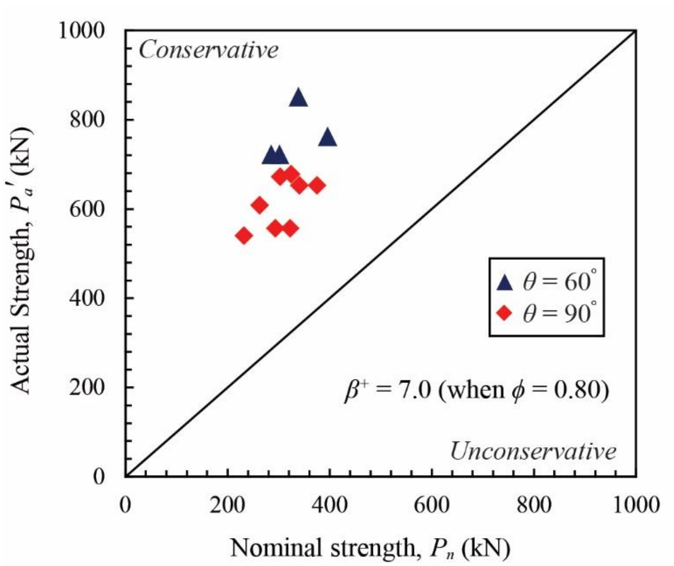

Fig. 15. Correlation of existing AWS [9] provisions with the test results, with weld effective lengths

If, instead, no effective length rules are applied, and the total weld length is used to determine the strength of the welded joint, then the correlation in Fig. 16 results. The implied safety index is then 4.9. The mean experimental-to-predicted strength is 1.42. As $\beta^{+} > 4.0$, it can be concluded that, for the range of parameters studied, weld effective lengths are not required in conjunction with the AWS [9] code design method evaluated.

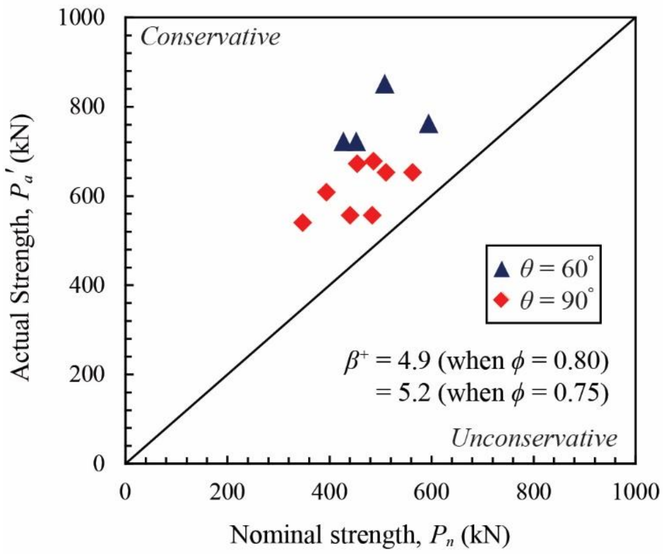

Fig. 16. Correlation of existing AWS [9] provisions (excluding weld effective lengths) and AISC [7] provisions with test results

5.3. Comparison to AISC [7] and CSA [26]

AISC [7] gives the same equations (Eq. 2a,b) for the nominal strength of fillet welds via Clause J.2.4a with $l_e = l_w$; however, to calculate the design strength, a resistance factor, ϕ = 0.75 (instead of 0.80), is used. The implied safety index, β^+, is equal to 5.2 for AISC Clause J.2.4a (Table 6 and Fig. 16), which is expectedly larger than the minimum target safety index of 4.0, and the implied safety index of 4.9 when AWS D1.1 is used without weld effective lengths. The foregoing evaluations of both the AWS and AISC fillet weld design provisions assume that the $(1+0.50\sin^{1.5}\theta)$ directional strength-enhancement factor is not used (AISC Clause J2.4b and AWS Clause 2.6.4.2), because it has been shown to be generally unsafe for the design of fillet welds in HSS connections [27].

The ultimate strength of fillet welds in the Canadian steel code, CSA S16 [26], is also based on the limit state of shear rupture along the weld effective throat; however, CSA gives a different equation than AWS and AISC for the nominal strength (P_n) of fillet welds (Clause 13.13.2.2):

$$P_n = 0.67 A_w F_{EXX} \tag{8}$$

where $A_w = t_w l_w$.

An LRFD resistance factor for fillet welds, ϕ, equal to 0.67, is then applied to determine the design strength. As discussed for AISC Clause J2.4b [7], the above equation also excludes the $1+0.50\sin^{1.5}\theta$ directional strength-enhancement factor.

CSA gives a higher nominal strength than AISC for fillet welds (0.67 versus 0.60 for the shear strength factor) and a proportionally lower resistance factor (ϕ = 0.67 versus 0.75). The reliability index, β^+, implied by CSA Clause 13.13.2.2 is therefore the same as β^+ implied by AISC Clause J.2.4a (β^+ = 5.2, which is greater than 4.5, the target safety index per Annex B of CSA [26]). Fig. 17 shows the correlation of the CSA predicted nominal strengths with the experimental results. On average, the experimental strength is only 1.27 times larger than that predicted with Eq. (8), using the measured values of A_w and F_{EXX}. This value is the closest to unity amongst all methods investigated (AWS with/without weld effective lengths, AISC, and CSA). Still, more work is needed to determine the effect of connection parameters outside of the range studied on the weld strength.

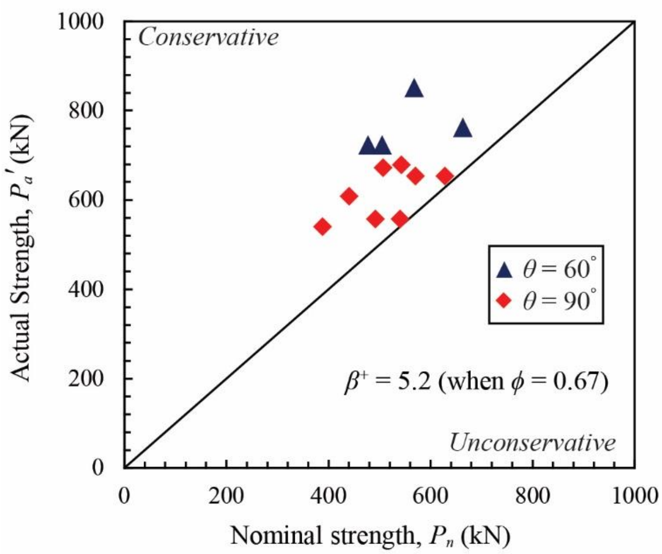

Fig. 17. Correlation of CSA [26] provisions with test results

5.4. Evaluation of AWS [9] total weld length approximations

In AWS [9], the total weld length is determined from the following equation (Clause 9.5.4):

$$l_w = \pi D_b K_a \tag{9}$$

where K_a = weld length factor, given as:

$$K_a = \frac{1}{2\pi\, sin\theta} + \frac{1}{3\pi}\left(\frac{3-\beta^2}{2-\ \beta^2}\right) + 3\sqrt{(\frac{1}{2\pi\, sin\theta})^2 + (\frac{1}{3\pi}\left(\frac{3-\beta^2}{2-\ \beta^2}\right))^2} \quad (10)$$

Eq. (10) gives the projection of the weld root along an inclined branch onto a cylindrical surface. It takes into account both the branch-angle and beta-ratio distortion of the weld length. If one considers a CHS branch welded to a flat plate at θ = 90°, with l_w then equal to πD_b, branch-angle distortion is the transformation of the circular weld into an ellipse caused by a change in θ. Beta-ratio distortion occurs when the flat plate is replaced by a cylindrical surface, causing the plane of the weld to distort into a saddle shape. Despite its complex appearance, Eq. (10) is only an approximation to the weld length. Note that when β equals zero and θ equals 90°, such as the case for welding a CHS branch at 90° to a flat plate in the example above, K_a does not equal exactly 1.00 using Eq. (10). Instead, it equals 0.99. Hence, as part of a comprehensive evaluation of the AWS code, it is necessary to evaluate the error associated with this method to calculate l_w.

Fig. 18 shows the relationship between $l_w/\pi D_b$ (= K_a) determined using Eq. (10) and $l_w/\pi D_b$ determined from the vector-calculus method, as used herein, for a range of β values. It is shown that Eq. (10) is conservative as a design tool, i.e. it under-predicts the weld length. The maximum error is only 0.6% over the range of parameters studied (for β = 0.10 and θ just less than 90°). Thus, despite its complexity, Eq. (10) gives a predicted weld length very close to the actual weld length.

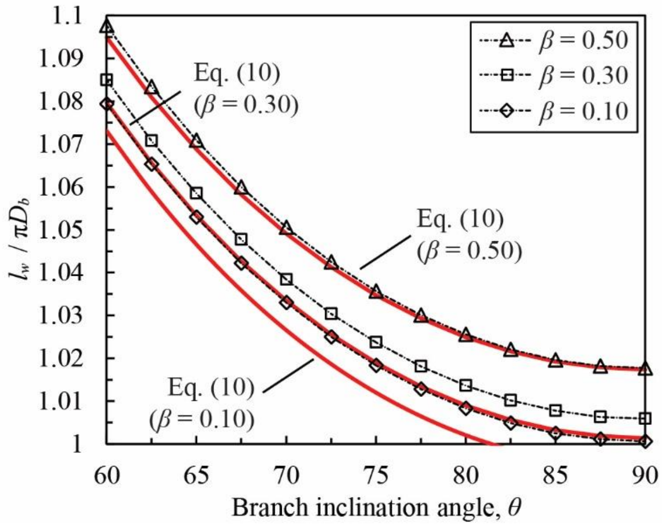

Fig. 18. Comparison of $l_w/\pi D_b$ using Eq. (10) (AWS [9]) and the vector-calculus method

AWS notes that the following formula for K_a may be conservatively used instead of Eq. (10) to calculate l_w for CHS connections:

$$K_a = \frac{1 + 1/\sin\theta}{2} \tag{11}$$

Fig. 19 (analogous to Fig. 18) shows the relationship between $l_w/\pi D_b$ determined using Eq. (11) and $l_w/\pi D_b$ determined from the vector-calculus method. It is shown that Eq.(11) is even more conservative than Eq. (10) as a design tool. The maximum error is still only 1.9% over the range of parameters studied (for β = 0.50 and θ = 90°), which is expectedly larger than the error associated with Eq. (10). However, Eq. (11) is always conservative.

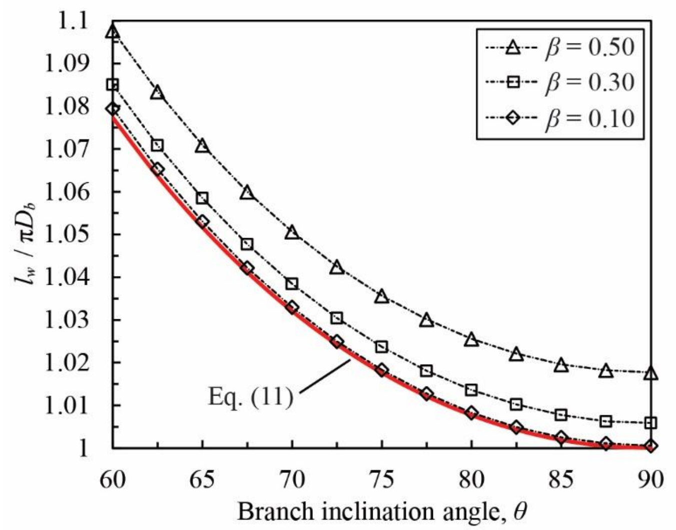

Fig. 19. Comparison of $l_w/\pi D_b$ using Eq. (11) (AWS [9]) and the vector-calculus method

One could argue that, since these lower-bound approximations give actual-to-predicted weld lengths greater than 1.00, mean values and variations in the actual-to-predicted weld length should be included in the factors ρ_G and V_G in the reliability analysis. Including these variations would marginally increase the reliability index (β^+). However, with CAD now widely used for design and analysis, it seems increasingly likely that designers will opt to find the total weld length using software, rather than using Eqs. (10) or (11). It was therefore deemed prudent to omit variations in the actual-to-predicted weld length in the factors ρ_G and V_G, because including them would be un-conservative. Eqs. (10) and (11) are still, however, useful (and conservative) design tools.

6. Evaluation of procedures to determine weld effective lengths for CHS from test results

For calculating weld effective lengths from tests, which have been shown to exist for CHS-to-CHS X-connections in Section 4, three methods are evaluated:

Method 1: The ratio of l_e to l_w is taken as the ratio of nominal-to-peak elastic strain. The nominal elastic strain was calculated by multiplying strain measured in the branch adjacent to the weld (as shown in Figs. 12a,b and 13a,b when $P = 0.25\ P_a$), by the weld length tributary to the measurement, then dividing the sum of the results by the sum of the tributary weld lengths. Since the strain is elastic, the result of using P_a' instead of P_a in this process is not significant. Either the entire weld length, or a length of weld between a plane or planes of symmetry, should be instrumented with SGs when using this method. Compressive strains in the branch adjacent to the weld were taken as zero strain (rather than negative strain), because they do not increase the weld effective length. Wang et al. [28] used this method to study weld effective lengths for CHS branch-to-RHS chord connections. Caulkins [29] used a similar method to study welds in CHS T-connections. His method used forces from finite element models instead of elastic strains. Due to proportionality, however, it yields the same results. The appeal of this method is that weld effective lengths can be determined from elastic tests, and it logically takes into account stress concentrations along the weld length. Moreover, weld-critical tests, which are difficult to achieve, are not needed. This method is based explicitly on elastic load/stress distribution, and it does not take into account load/stress re-distribution in the weld before rupture. It is therefore likely to be a lower-bound.

Method 2: the weld effective length is empirically determined by comparison of actual-to-predicted strengths, with P_n calculated using an accurate predictor such as Eq. (12), with actual values of t_w, t_b, D_b, A_w, and F_{EXX} [30]:

$$P_n = \left(1.009 - 0.00137\frac{D_b}{t_b} - 0.197\frac{t_w}{t_b}\right) A_w F_{EXX} \tag{12}$$

Eq. (12) was developed from regression of a large database of weld-critical CHS-to-rigid end-plate connection finite element results [30]. As such, it is tailored to the unique loading on single-sided fillet welds to CHS branches (which produces tension at the weld root under branch axial tension), and moreover takes into account the principal influential geometric parameters of the CHS member and weld joint. It is used to predict the strength of a fillet weld to a CHS branch when the weld is fully effective (i.e. $l_e = l_w$). The ratio of l_e to l_w for each test is hence the ratio of P_a' (Table 1) to the predicted value using Eq. (12). Method 2 takes into account load/stress re-distribution in the weld before rupture, unlike Method 1. It also utilizes an accurate formula for predicting the nominal weld strength [Eq. (12)]. Since Eq. (12) was developed from extensive testing and finite element analysis on CHS connections, Method 2 is believed to be the most accurate way to determine the true weld effective lengths.

Method 3: the weld effective length is empirically determined by comparison of actual-to-predicted strengths, with P_n calculated using Eqs. (2a,b), with $l_e = l_w$ and actual values of t_w, l_w, and F_{EXX}. The ratio of l_e to l_w is hence the ratio of P_a' (Table 1) to the predicted nominal weld strength using simple code equations. Method 3 provides the values of l_e for each fillet weld that would result in an actual-to-predicted strength ratio of 1.0 when used in conjunction with the AWS [9] fillet weld design provisions [Eqs. (2a,b)], and also the AISC [7] fillet weld design provisions in Clause J2.4a.

Table 7 gives the values of l_e/l_w computed for each of the 12 fillet welds in the CHS X-connections tested herein, using Methods 1 to 3.

Table 7
Weld effective length ratios determined using three possible methods

	Weld effective length ratio, l_e/l_w		
Test	Method 1	Method 2	Method 3
102-273-90a	0.29	1.01	1.48
102-273-90b	0.29	0.96	1.39
102-406-90a	0.28	1.03	1.54
102-406-90b	0.28	1.03	1.55
127-273-90a	0.28	0.82	1.28
127-273-90b	0.28	0.75	1.16
127-406-90a	0.27	0.81	1.26
127-406-90b	0.27	0.74	1.15
102-406-60a	0.33	1.13	1.69
102-406-60b	0.33	1.08	1.59
127-406-60a	0.32	0.83	1.28
127-406-60b	0.32	1.07	1.67

With Method 1, l_e/l_w is always less than 1.0, and moreover much less than 2/3 [Clause 9.6.1.3(4) of AWS [9]]. Since $l_e = (2/3)l_w$ has already been shown to be very conservative (Section 5.2), it can be concluded that Method 1 is even more conservative and inaccurate. The aim in assessing the values of l_e/l_w in Table 7 is to achieve a weld effective length ratio between 2/3 and 1.0.

With Method 2, l_e/l_w is between 0.75 and 1.13 (Table 7). Generally, fillet welds in connections with similar parameters (β, D/t, τ) have similar ratios of l_e/l_w, in accordance with expectations based on previous research [29].

For Method 3, using Eqs. (2a,b), the weld effective length is always greater than the real length, which cannot be true. This outcome is not unexpected, since Eq. (2) (and AISC [7] Clause J2.4a) has already been shown to be conservative for CHS connections with fully effective welds [30].

Method 2 is therefore a logical procedure to determine weld effective lengths from tests. It is thus deduced that weld effective lengths for CHS vary as a function of connection parameters, and rupture tests (experimental and/or numerical) over a broad range of geometric parameters are necessary to reasonably determine weld effective lengths.

7. Conclusions

Based on 12 careful laboratory tests on CHS X-connections under branch axial tension, which all failed by rupture along a plane through the connecting fillet weld, it is shown that weld effective lengths exist in CHS-to-CHS connections, and that the existing AWS code provisions for weld effective lengths in such connections, given by Clause 9.6.1.3(4), are very conservative. Furthermore, it is shown that the current AWS, AISC, and CSA specification provisions provide adequate structural reliability ($\beta^{+} \geq 4.0$ or 4.5) without weld effective lengths (i.e. using the total weld length to determine the weld strength), assuming the fillet weld directional strength enhancement factor is not used. This is due to the simplicity of the fillet weld nominal strength formula, because weld lengths were shown (by strain distributions) to be less than 100% effective. These conclusions are currently limited to $0.25 \leq \beta \leq 0.47$, $23 \leq D/t \leq 34$, $0.6 \leq \tau \leq 1.0$ and $\theta = 60°$ or $90°$.

A systematic approach to calculating the total weld length in CHS-to-CHS connections has also been presented. This approach is based on vector calculus and can be easily programmed to allow designers, fabricators, and researchers of tubular structures to accurately calculate weld lengths. The approximations given in AWS [9] Clause 9.5.4 for the total weld length (l_w) in CHS connections were compared to the vector-calculus approach and found to be useful lower-bound design tools for connections with $0.1 \leq \beta \leq 0.5$ and $60° \leq \theta \leq 90°$.

It is shown that the ratio of the weld effective length to the total weld length (l_e/l_w) is not constant for all CHS connections, as the current AWS specification currently implies via Clause 9.6.1.3(4), and varies as a function of connection parameters. It is also concluded that rupture tests on weld-critical connections are necessary to reasonably determine weld effective lengths.

A comprehensive parametric modelling study, using finite element methods, and a secondary reliability analysis are presented in a Part II companion paper which investigates: (a) if these findings are applicable to a wider range of fillet-welded CHS X-connections, and (b) the effect of connection parameters β, θ, D/t, and τ on the weld strength.

Acknowledgements

Financial support for this project was provided by the Natural Sciences and Engineering Research Council of Canada (NSERC). CHS sections were donated by Atlas Tube, Harrow, Canada, and in-kind fabrication services were provided by Walters Inc., Hamilton, Canada. The Authors gratefully acknowledge the laboratory assistance of Mr. Fei Wei.

Notation

A_w	weld throat area (= $t_w l_w$)
A_b	cross-sectional area of the branch
A	cross-sectional area of the chord
D	diameter of the chord
D_b	diameter of the branch
E	Young's modulus
F_{EXX}	ultimate strength of weld metal
F_y	yield strength
K_a	weld length factor
P	applied load
P_a	actual (experimental) weld fracture load
P_a'	greatest load sustained by the weld
$\vec{P}_i$	position vector at point i along the branch-chord intersection
P_n	nominal predicted weld fracture load
Q_w	shear strength of weld per unit length
$\vec{V}$	approximation to the weld length between two points along the weld
V_G	coefficient of variation of ρ_G
V_M	coefficient of variation of ρ_M
V_P	coefficient of variation of ρ_P
V_R	coefficient of variation of ρ_R
i	symbol denoting ρ or $\rho + \Delta\rho$
l	length of the chord

l_b	length of the branch
l_e	weld effective length
l_h	weld leg along the chord
l_t	template length parallel to branch
l_v	weld leg along the branch
l_w	total length of weld
t	thickness of the chord
t_b	thickness of the branch
t_w	weld throat dimension
x	distance between the collar and the weld toe along the branch
α_R	coefficient of separation
β	branch-to-chord diameter ratio
β^+	safety index
$\Delta\rho$	subtended angle increment
ε_{rup}	elongation at rupture
δ	chord deformation
δ_a	actual (experimental) chord deformation at rupture
ρ	subtended angle around the branch, measured from heel
ρ_G	mean ratio of measured-to-nominal weld throat area
ρ_M	mean ratio of measured-to-nominal electrode ultimate strength
ρ_P	mean test-to-predicted capacity ratio
ρ_R	bias coefficient for resistance
τ	branch-to-chord thickness ratio
ϕ	LRFD resistance factor for fillet welds
$\phi_{\beta}{}^{+}$	adjustment factor for β^+
θ	branch inclination angle
Ψ	local dihedral angle

References

[1] ISO (International Organization for Standardization). 2013. ISO 14346:2013 (E). Static design procedure for welded hollow section joints – Recommendations, Geneva, Switzerland.

[2] Frater, G. S. & Packer, J. A. 1992. Weldment design for RHS truss connections. I: Applications. *Journal of Structural Engineering, American Society of Civil Engineers* 118(10): 2784-2803.

[3] Frater, G. S. & Packer, J. A. 1992. Weldment design for RHS truss connections. II: Experimentation. *Journal of Structural Engineering, American Society of Civil Engineers* 118(10): 2804-2820.

[4] Packer, J. A. & Cassidy, C. E. 1995. Effective weld length for HSS T, Y, and X connections. *Journal of Structural Engineering, American Society of Civil Engineers* 121(10): 1402-1408.

[5] McFadden, M. R. & Packer, J. A. 2014. Effective weld properties for hollow structural section T-connections under branch in-plane bending. *Engineering Journal, American Institute of Steel Construction* 51(4): 247-266.

[6] Tousignant, K. & Packer, J. A. 2015. Weld effective lengths for rectangular HSS overlapped K-connections. *Engineering Journal, American Institute of Steel Construction* 52(4): 259-282.

[7] American Institute of Steel Construction (AISC) 2016. ANSI/AISC 360-16. Specification for structural steel buildings. Chicago, IL, USA.

[8] Marshall, P.W. 1992. Design of welded tubular connections – Basis and use of AWS code provisions. Amsterdam, The Netherlands: Elsevier.

[9] American Welding Society (AWS) 2015. AWS D1.1/D1.1M:2015. Structural welding code—steel. Miami, FL, USA.

[10] ASTM International 2013. ASTM A500-13. Standard specification for cold-formed welded and seamless carbon steel structural tubing in rounds and shapes. West Conshohocken, PA, USA.

[11] ASTM International 2017. ASTM A370-17. Standard test methods and definitions for mechanical testing of steel products. West Conshohocken, PA, USA.

[12] Luyties, W. H. & Post, J. W. 1988. Local dihedral angle equations for tubular joints and related applications. *Welding Journal* 77(4): 51-60.

[13] Mehrotra, B. L. & Govil, A. K. 1972. Shear lag analaysis of rectangular full-width tube connections. *Journal of the Structural Division, American Society of Civil Engineers* 98(ST1): 287-305.

[14] Packer, J. A. & Henderson, J. E. 1997. Hollow structural section connections and trusses - a design guide. 2nd ed. Toronto, Canada: Canadian Institute of Steel Construction.

[15] van der Vegte, G.J. & Makino, Y. 2010. Further research on chord length and boundary conditions of CHS T- and X-joints. *Advanced Steel Construction* 6(3): 879-890.

[16] Lie, S. T., Lee, C. K. & Wong S. M. 2001. Modelling and mesh generation of weld profile in tubular Y-joint. *Journal of Constructional Steel Research* 57(5): 467 - 580.

[17] Packer, J. A., Choo, Y. S., Shen, W., Wardenier, J., van der Vegte, G. J., & Mustard, T. 2012. CIDECT Report 5BW-2/12. Axially loaded T and X joints of elliptical hollow sections. Geneva, Switzerland: CIDECT.

[18] Lu, L. H., de Winkel, G. D., Yu, Y. & Wardenier, J. 1994. Deformation limit for the ultimate strength of hollow section joints. In Paul Grundy, Alan Holgate and Bill Wong (eds.), *Tubular Structures VI; Proc. Intern. Symp., Melbourne 14-16 December 1994.* Rotterdam: Balkema, 341-348.

[19] British Standards Institution (BSI) 1959. BS 449:1959. Specification for the use of structural steel in building. London, England.

[20] Ravindra, M. K. & Galambos, T. V. 1978. Load and resistance factor design for steel. *Journal of the Structural Division. American Society of Civil Engineers* 104(9): 1337-1353.

[21] Fisher, J. W., Galambos, T. V., Kulak, G. L. & Ravindra, M. K. (1978). Load and resistance factor design criteria for connectors. *Journal of the Structural Division, American Society of Civil Engineers* 104(9): 1427-1441.

[22] Franchuk, C. R., Driver, R. G. & Grondin, G.Y. 2002. Block shear failure of coped steel beams. *Proc. Annual Conf. of the Canadian Society for Civil Engineering, Montreal, 5-8 June 2002*. 1000-1009.

[23] Tousignant, K. & Packer, J. A. 2016. Experimental evaluation of directional strength-enhancement factor for fillet welds to CHS. *Connections VIII; Proc. Intern. Workshop on Connections in Steel Structures, Boston, 24-25 May 2016*.

[24] Lesik, D. F. & Kennedy, D. J. 1990. Ultimate strength of fillet welded connections loaded in plane. *Canadian Journal of Civil Engineering* 17(1): 55-67.

[25] Callele, L. J., Driver, R. G. & Grondin, G. Y. 2009. Design and behavior of multi-orientation fillet weld connections. *Engineering Journal, American Institute of Steel Construction* 46(4): 257-272.

[26] Canadian Standards Association (CSA) 2014. CSA S16-14. Design of steel structures. Toronto, Canada.

[27] Packer, J. A., Sun, M., & Tousignant, K. 2016. Experimental evaluation of design procedures for fillet welds to hollow structural sections. *Journal of Structural Engineering, American Society of Civil Engineers* 142(5): 04016007-1 – 04016007-12.

[28] Wang, W., Gu, Q., Ma, X. & Wang, J. 2015. Axial tensile behavior of welds for CHS branches to SHS chord joints. *Journal of Constructional Steel Research* 115: 303-315.

[29] Caulkins, D. W. 1968. CDG Report 15. Parameter study for FRAMETI elastic stress in tubular joints. Houston, TX, USA: Shell Oil Company.

[30] Tousignant, K. & Packer, J. A. 2017. Numerical investigation of fillet welds in HSS-to-rigid end-plate connections. *Journal of Structural Engineering, American Society of Civil Engineers,* in press.

Figure Captions

Fig. 1. Variation of X-connection stress distributions

Fig. 2. Connection layout

Fig. 3. Local dihedral angle curves for test joints, with subtended angle measured from the crown heel

Fig. 4. Fit-up of branch to chord after profiling and tack welding

Fig. 5. Vector calculus method used to determine weld lengths

Fig. 6. 3D Solidworks models of weld profile and weld dimensions

Fig. 7. Typical testing arrangement (shown for test 127-273-90a)

Fig. 8. Strain gauges near weld toe (and weld fracture) in test 127-273-90a

Fig. 9. Typical weld fractures

Fig. 10. Typical load versus chord deformation relationships

Fig. 11. Procedure for calculating load versus deformation for second welds tested

Fig. 12. Typical strain distributions adjacent to test weld (θ = 90° connections)

Fig. 13. Typical strain distributions adjacent to test weld (θ = 60° connections)

Fig. 14. Effect causing compressive strains at the crown (ρ = 0° and 180° points) (θ = 90° connections)

Fig. 15. Correlation of existing AWS [9] provisions with the test results, with weld effective lengths

Fig. 16. Correlation of existing AWS [9] provisions (excluding weld effective lengths) and AISC [7] provisions with test results

Fig. 17. Correlation of CSA [26] provisions with test results

Fig. 18. Comparison of $l_w/\pi D_b$ using Eq. (10) (AWS [9]) and the vector-calculus method

Fig. 19. Comparison of $l_w/\pi D_b$ using Eq. (11) (AWS [9]) and the vector-calculus method